Experiments with an Automated Visual Inspection System

Eugene C. Chalfant Bruce Bon Won S. Kim
Jet Propulsion Laboratory
California Institute of Technology
4800 oak Grove Drive
Pasadena, CA 91109

Abstract

Experiments were performed with an automated visual inspection system that detects potential flaws by comparing reference and comparison images. Three main components evaluated are: 1) image-differencing-based ambient light compensation, 2) electronic-shuttering-based ambient light rejection, and 3) image registration. The results indicate that the ambient light compensation algorithm yields 0.01% to 0.4% false flaws with lab-simulated sunlight changing from 25% to 100% intensity. Electronic shuttering with synchronized strobe lighting reduces false flaws considerably. As exposure Shortens from 1/60 (fully open) to 1/1000 second, false flaws decrease 100-fold from 0.4% to O. 004%. The current registration algorithm corrects a very limited range of misregistration, correcting approximately 4 pixels of pure translational shifts over the inspection surface. A more robust image registration algorithm that can correct both translational and rotational shifts over 10 pixels misregistration would be highly desirable,

Keywords: vision, automated inspection, ambient light compensation, image differencing, registration

1 Introduction

Automated robotic inspection of space platforms such as the International Space Station is expected to be an important element to offload time-consuming inspection activities from astronauts [I]. The Jet Propulsion Laboratory recently developed such a remote surface inspection (RSI) system, and demonstrated it successfully on the ground in a constrained lab environment [2][3][4]. The JPL RS1 system developed through 1995 is described in detail in [4]. Further enhancements made in 1996 together with performance evaluation experiments are described in [5].

The system supports four types of inspection: 1) automated visual inspection, 2) eddy current sensor based surface crack inspection, 3) temperature inspection, and 4) gas leak inspection. our emphasis in 1996 has been to enhance the automated visual inspection capability for more robust flaw detection and to evaluate its performance. The enhanced RSI system has been delivered to the NASA Johnson Space Center Automated Robotic Maintenance of Space Station (ARMSS) facility for on-site test and technology demonstration of remote surface inspection capabilities to the Space Station Program.

This paper describes experiments with this enhanced automated visual inspection system. Section 2 describes the JPL Automated Inspection System in more detail. Section 3 describes the 2-D and 3-I) flaw detection process. Sections 4, 5, and 6 present experimental results on ambient light compensation, electronic shuttering, and image registration, respectively. Section 7 describes operational experiments that were conducted. Finally, Section 8 discusses the system limitations and desired future enhancements.

2 JPL Automated Visual Inspection System and Enhancements

Visual inspection and flaw detection is a critical and labor-intensive maintenance task, particularly in hazardous environments such as space. One particularly useful application of this technology to reduce workload is the inspection of the exterior of the International Space Station fox damage due to micrometeorites, orbital debris, or corrosion from atomic oxygen,

In on-orbit space applications such as Space Station surface inspection, the ambient lighting conditions may change drastically due to sun orientation changes. When reference and comparison images are taken under different ambient lighting conditions, a simple image differencing will generate too many fake alarms due to changes in shading. A simple but impractical solution to this problem is to block ambient light completely and use only the controlled lights (e.g., strobe lights) mounted on the robot arm end effector. A clever practical solution that achieves tbe same effect is the ambient light compensation process developed and implemented for the JPL automated visual inspection system [3]. First, the surface image is taken with the controlled lights on, and immediately thereafter the image is taken again with the lights off. The differencing of the two images results in a compensated "controlled light only" image that appears as if there were no ambient lighting. The automated visual inspection uses the compensated reference and comparison images to detect changes as potential flaws by image differencing.

The imaging system of the JPL automated inspection system consists of cameras, strobe lights, an image processor, and a simulated sunlight source. Two color CCD cameras with electronic shuttering (Toshiba IK-M41A) and two strobe lights (EG&G MVS5000) are mounted on the end of a seven-dof Robotics Research Corporation arm as part of an integrated multi-sensor end effector. The entire robot arm is mounted on a 1-dof mobile rail platform. The computer-controllable strobe light is synchronized with the electronic shuttering to reduce ambient light energy to 1/16th of the unshuttered amount while still capturing the entire strobe pulse. Simulated sunlight is provided at one-tenth orbital intensity by a 1.5 kW xenon arc lamp on a pan-tilt-rail mount.

The real-time software for manipulator control and automated visual inspection resides in a VME chassis, running on the VxWorks real-time operating system. A Datacube MaxVideo-200 board with a mini-warper is used for real-time image processing.

Software to control the remote-site inspection system from the local-site operator control station (housed in a Space Station cupola mockup) includes a graphical user interface which allows the user to define and modify inspection paths, catalog detected flaws, move the robot arm interactively, and execute predefined scripts. The operator may also inspect the mockup by manually teleoperating the arms if desired. A 3-D graphical simulation of the testbed and a video monitoring system help to provide the operator with situational awareness without a direct view.

The operator interface has been enhanced by incorporating command scripts to support three operational modes for visual inspection: quasi-static human visual inspection, quasi-static automated visual inspection, and continuous-motion automated visual inspection. A reference image display window has been added to facilitate the operator's image comparison for flaw marking decisions.

3 Flaw Detection

An inspection taskboard (Figure 1) was designed for the experiments. It incorporates a resolution test pattern and a variety of surface relief features and small structures such as standoffs to create complex shadows. The inspection taskboard consists of three pairs of panels: flat 2-D, concave holes (bare metal and painted)/convex bumps, and 3-D structure sections. The bottom right panel is silk-screened with a 2-D test pattern for measuring inspection resolution by detecting test "flaws" of various sizes, shapes, and patterns. Simulated flaws, for example black, grey, or colored tape patches, can be added to the 3-D panels prior to inspection experiments.

Experiments with the 2-D test pattern indicate that the minimum detectable flaw size at a distance of approximately 29 cm was between 0.3 and 2.5 mm, depending on the shape and orientation of the flaw, as shown in Table 1. Low contrast flaws were not detected

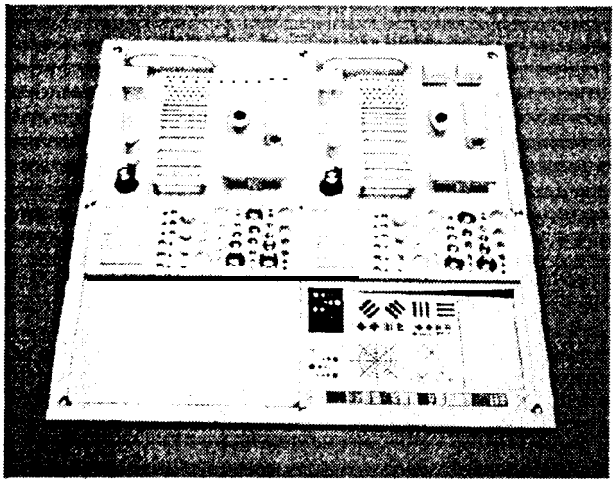

Figure 1: Taskboard showing 3-D structures and 2-D test pattern

Test	Smallest flaw detected, mm	pixels
1. long, thin horiz triangle	0.5 mm	1.0
2. line detection - horiz	0.3 mm	0.6
vertical	0.3 mm	0.6
45 degree	0.3 mm	0.6
3. black-on-white dots	2.5 mm	5.0
4. gray-on-white dots	none	none

Table 1: 2-D flaw detection results using full intensity sun lamp

Flaw detection for the three dimensional surfaces of the inspection taskboard is illustrated in Figures 2-4, Figure 2 shows a raw image of the taskboard containing no flaws, illuminated by full intensity simulated sunlight, used as the reference image. Figure 3 shows a raw comparison image containing flaws simulated by pieces of black tape. The illumination was reduced to 50% using a neutral density filter for this comparison image. Figure 4 shows the flaws detected after ambient light compensation and image differencing.

Although the ambient light level was changed drastically, the automated visual inspection system correctly detects the actual flaws. Note, however, that some false flaws were generated due to imperfect ambient light compensation. A robust inspection system should minimize false flaws under any lighting and misregistration conditions. In our experiments, the percentage of pixels indicated as false flaws was used to quantify performance of the system. A perfect inspection system, of course, would detect no false flaws.

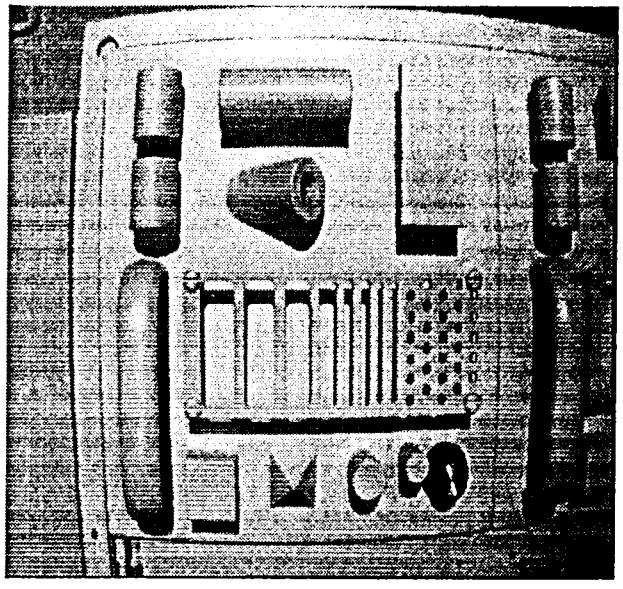

Figure 2: Raw reference image with 100% ambient light illumination

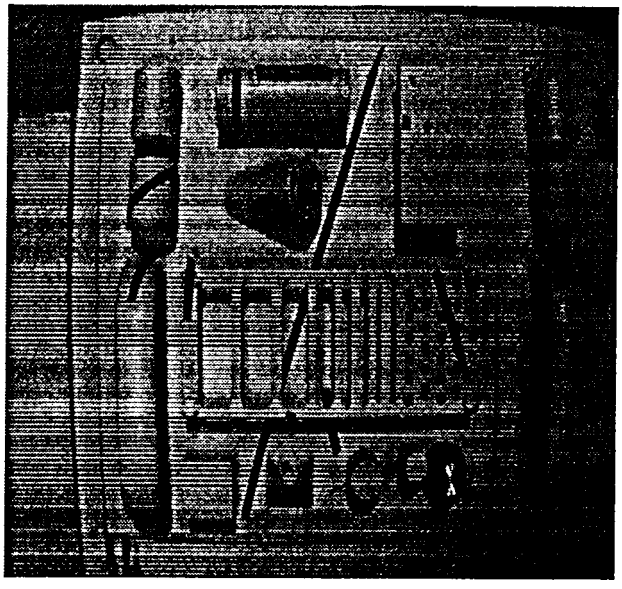

Figure 3: Raw comparison image with 50% ambient light illumination

4 Ambient Light Compensation

Ambient light compensation is performed by subtracting an ambient-light-only image from a strobe + ambient lit image. These images are sampled from an interlaced scan CCD video camera, The video camera generates 30 complete frames per second. Each frame consists of two fields of alternate scan lines. The strobe duration is approximately 20 microseconds, so only one field (i.e., every other scan line) is illuminated by the strobe. The raw image is a complete frame Consisting of interlaced strobe + ambient and ambient-only lines. The two half-resolution fields are differenced, resulting in a half-resolution image which appears as if illuminated only by the strobe.

Differencing of the raw images to generate a compensated image requires that the pixel intensity of the digitized image be linear with respect to the incident light energy. Video cameras typically incorporate gamma correction designed to compensate for the nonlinear response of the human eye. Linearity is restored in our inspection system via a calibration lookup table. Also, automatic gain control is disabled.

The performance of ambient light compensation was evaluated by acquiring reference and comparison images of identical surfaces under different conditions of incidence angle and intensity. Any flaws detected are the result of imperfect compensation. Electronic shuttering was disabled for this experiment in order to evaluate ambient light compensation in isolation. Figure 5 snows an ambient light compensated image. The compensation process results in a half resolution image that is relatively dark. Faint ghost outlines of the removed shadows can be seen - these are eliminated when electronic spluttering is used. Figure 6 shows tile false flaws detected when the reference image was taken at 0% intensity (dark) and the comparison image taken at 100% intensity, the worst case. Figure 7 plots the increase in the number of false flaws as the difference in illumination intensity between the reference and comparison images increases.

5 Electronic Shattering

An electronic shutter that controls the CCD charge integration time can help reject ambient light by minimizing the ambient light energy reaching the CCD, without diminishing the strobe light energy. Using the electronic shutter requires careful synchronization of the video shutter with the strobe light.

Figure 6 shows false flaws detected using a reference image with no ambient illumination and a comparison image with 100% ambient illumination at full open shutter (16.7 ms). The false flaws occur at the edges of ambient light shadow's and at bright specular highlights. Figure 8 shows the improvement garnered by using a shutter duration of 1 rms. All the false flaws at the shadow edges have been eliminated. Figure 9 shows the reduction in the percentage of fake flaw pixels as shutter duration is decreased.

The new electronic shuttering with synchronized strobe lighting drastically reduces fake flaw generation. As the shutter open duration decreases from 1/60 s (continuous exposure) to 1/1000 s (1/16 exposure), the false flaw yield percentage decreases from 0.4% to 0.004 %, respectively. This result demonstrates a dramatic 100-fold reduction of false flaws by using a 1 /1000 s shutter speed.

Figure 4: Flaw blob image with 50% ambient light illumination

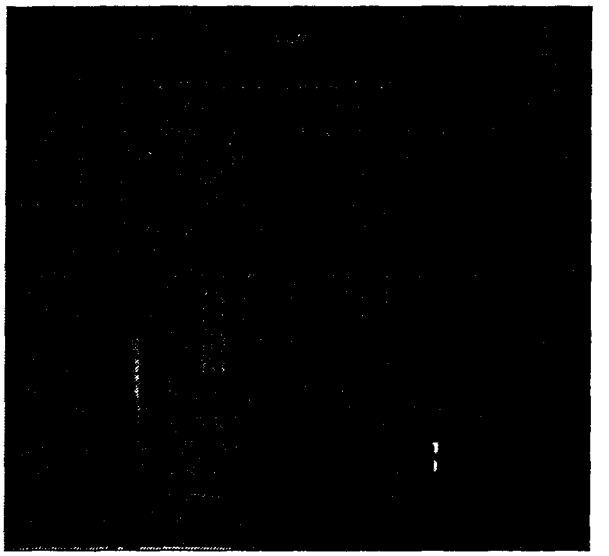

Figure 5: Ambient light compensated image

6 Image Registration

Flaw detection requires a reference image which may have been acquired some time before the comparison image. Due to repeatability errors in positioning the robot arm which holds the camera, the views may differ somewhat. Registration of the two views is therefore necessary to avoid false flaws.

Our visual surface inspection process uses an iterative fitting algorithm to correct misregistration parallel to the image plane. Low-pass blurring filters of various sizes are used to implement a mult i-resolution minimization technique. Misregistration due to errors in orientation or scaling are not corrected.

Results indicate that the current image registration algorithm corrects up to about 4 pixels of pure translational shifts of video images. In practical situations, the repetitive positioning precision of a robot end effector equipped with an inspection camera is limited, resulting in a slight positioning variation in all six degrees of freedom. Tests show that the cur- r cut 2-degree-of-freedom image registration algorithm is only marginally effective, and must be extended to handle all six degrees of freedom for more robust image registration.

Figure 10 plots the performance of the registration algorithm. After a reference image was acquired, the taskboard was moved by a stepper motor in increments of 0.05 mm, resulting in an image shift of about 1 /10 pixel. The flaw detection algorithm ignores flaws smaller than about 1.5 pixels in sire, and the regist ration algorithm corrects misregistration to a maximum of about 2.5 pixels. The system is tolerant of misregist rations of up to about 4 pixels (about 2 mm when the camera is about 29.5 cm away). Note that the algorithm consistently undercorrects misregistrations even smaller than 2.5 pixels.

7 operational Experiments

After the system component level experiments, operational level experiments were performed to compare three modes of operations: quasi-static human visual inspection, quasi-static automated visual inspection, and continuous-motion automated visual inspection. Due to time limitations, only very preliminary experiments have been performed. Preliminary trial runs suggest that the current image registration algorithm needs substantial enhancements.

8 Discussion

Our experimental results indicate that the automated visual inspection system could be an able assistant to human visual inspection for periodic maintenance inspection of the International Space Station. The automated visual inspection system could save a considerable amount of human visual inspection time if the new surface flaws are very few and over a large inspected surface area. The automated visual inspection system could also point to potential flaws that the human operator might have missed inadvertently.

The inspection system is limited by the quality of the video images. Ambient light compensation, as currently implemented, reduces the resolution of the image by 50% as well as reducing the intensity. The low intensity images are very susceptible to noise.

Saturation of the CCD causes intensity nonlinearity in the raw images which can result in false flaws being detected in bright areas, especially in specular reflections. Sat urat ion is curr ently avoided by using a manually operated mechanical iris to attenuate the

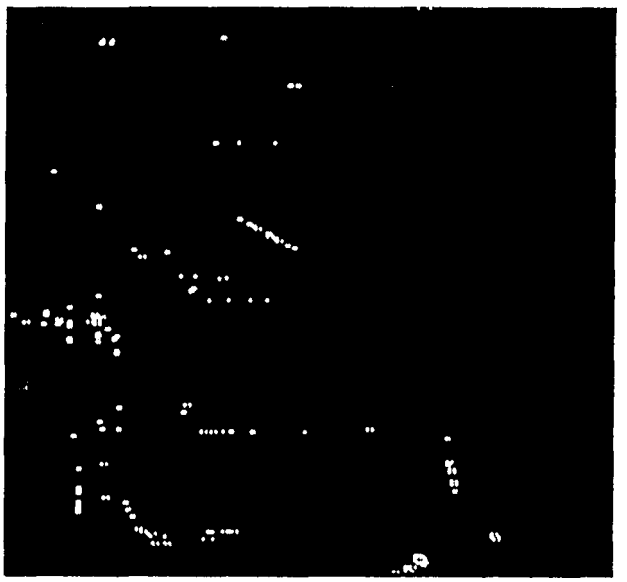

Figure 6: False flaws caused by illumination intensity change.

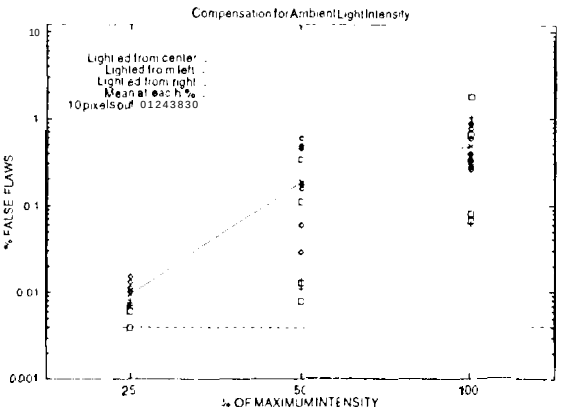

Figure 7: Percentage flaw pixels in flawless images for different intensities. Reference image was not illuminated by ambient light.

intensity of the scene. However, this also decreases the sensitivity of the camera in dim illumination. Linearizing the response of the camera also effectively reduces the dynamic range of the image.

The system generates false flaws due to rotational misregistration, which is not corrected by the registration algorithm. It is also very sensitive to misregistrations due to positioning errors perpendicular to the inspected surface (i.e., scaling misregistration).

The automated visual inspection developed so far needs further enhancements for practical use in the Space Station. Three major enhancements desired are listed line.

1 The current image registration algorithm has a very limited range of image registration capability. It can correct only approximately 4 pixels of translational shifts over the inspection surface. Since the accurate positioning of a robot arm equipped with an inspection camera is difficult, a more robust image registration algorithm that can correct both translational and rotational shifts over 10 pixels mis-registration is highly desirable.

2 The current strobe light has a fixed light energy level. A computer-controlled strobe light energy control to adjust the strobe light energy level depending upon surface properties is desirable in order to make automated visual inspection work properly over different surfaces with appropriate light intensity levels for strobe-lit video images. In conjunction, other techniques to increase or adapt the dynamic range of the camera are needed.

3. The current system uses teleoperation to generate a scan path for visual inspection. It assumes an accurate repeatable positioning of a robot arm base running on a mobile platform. In the actual Space Station environment, this may not be the case, and an initial camera positioning procedure may be necessary that is sufficiently accurate and repeatable, for example, by using the 3-D model-based virtual reality calibration technique [6].

9 Conclusion

We have evaluated the performance of an automated visual inspection system. Electronic shuttering was shown to be a highly effective method for rejecting ambient light. The operational limitations of each component of the system were presented. our results show that flaw detection performs well under certain conditions. Further work is required to make the system robust under arbitrary ambient lighting, conditions and larger camera positioning errors.

10 Acknowledgments

This work was performed at the Jet Propulsion Laboratory, California Institute of Technology, under contract with the National Aeronautics and Space Administration.

References

[1] F. Fisher and C. R. Price, "Space Station Freedom external maintenance task team final report," tech. rep., NASA Johnson Space Center, Houston, TX, July 1990.

[2] S. Hayati, J. Balaram, H. Seraji, W. S. Kim, and K. S. Tso, "Remote surface inspection sys-

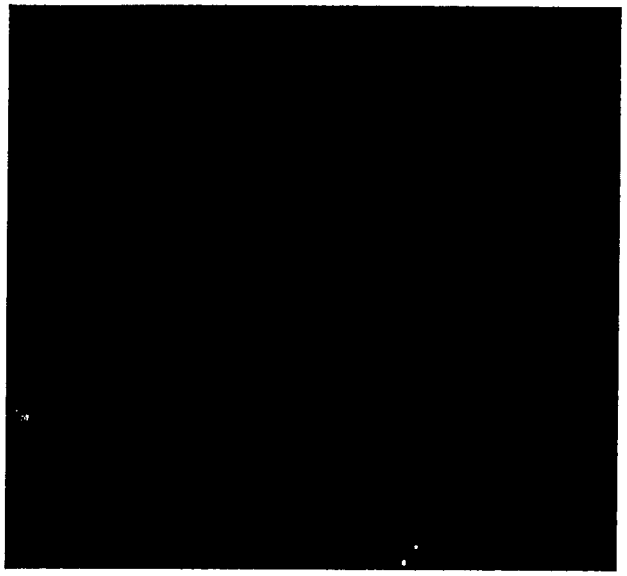

Figure 8: False flaws derived from image taken with 1 ms exposure.

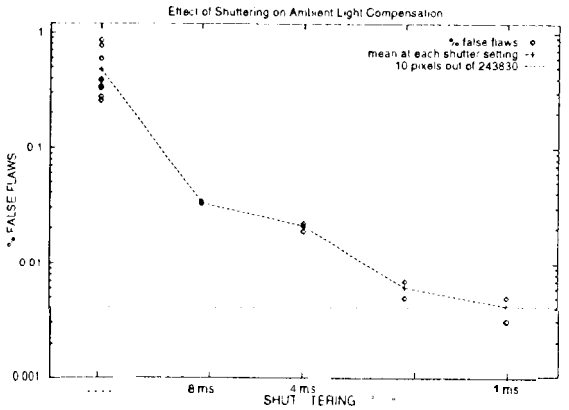

Figure 9: Percentage false flaw pixels for different shutter exposures.

tem," *Robotics and Autonomous Systems*, vol. 1 1, pp. 45-59, May 1993.

[3] J. B. Balaram, "Automated visual change detection for remote surface inspection." 49 pages, appears as Appendix E iu reference [4], 1993.

[4] P. G. Backes, J. B. Balaram, S. Hayati, W. S. Kim, T. Lee, D. Lim, H. Seraji, R. Steele, G. Tharp, and R. Volpe, "Remet e surface inspection system - fy'95 final report," Tech. Rep. JPL D-13446, Jet l'repulsion Laboratory, Pasadena, California, November 1995.

[5] M'. S. Kim, R. Steele, K. Tso, E. Majani, E. Barlow, B. Bon, E. Chalfant, "Remote Surface Inspection System Manuals and Experiments", Tech. Report JPL D-14083, Jet Propulsion Laboratory, Pasadena, California, December 1996.

[6] W. S. Kim, "Virtual reality calibration and preview/predictive displays for telerobotics", *Presence*, vol. 5, no. 2, pp. 173-190, 1996.

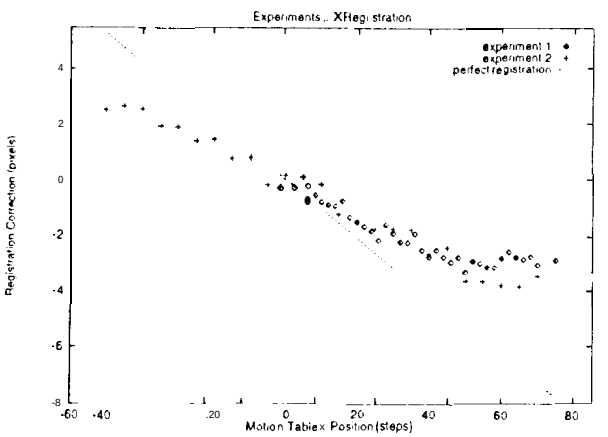

Figure 10: Horizontal registration correction versus measured registration error